High-efficient Nonlinear Control for Brushless Doubly-Fed Induction Machines

Hamidreza Mosaddegh Hesar, Xiaodong Liang, *Senior Member, IEEE*, Hossein Abootorabi Zarchi, Hamed Chenarani, and Amir Khazaee

***Abstract*--The brushless doubly-fed induction machine (BDFIM) is suitable for applications that need adjustable speed within limited ranges. It is a promising machine if its control strategies, such as the maximum torque per total copper losses (MTPCL) control, are well designed. A BDFIM has two stator windings, a power winding (not controllable) and a control winding (CW) (controllable through a partially rated back-to-back converter). Unlike singly-fed electrical machines, which are fully controllable and the MTPCL can be easily implemented to them, implementing the MTPCL control in a BDFIM is challenging. In this paper, the model-based MTPCL control strategy in the presence of a nonlinear controller in the BDFIM drive is developed. To realize this strategy, we first determine an expression in terms of the angle of the CW's current as a controllable variable. The optimal angle of the CW's current, which guarantees the realization of the MTPCL strategy, is then mathematically obtained using the numerical minimization approach. Next, the proposed passivity-based nonlinear controller regulates both the MTPCL criterion and the electromagnetic torque directly as the output variables. The proposed strategy is validated by a TMS320F2833 microcontroller synchronized with a personal computer for a 3 kW prototype D132s-BDFIM.**

***Index Terms*--Brushless doubly-fed induction machine (BDFIM), current angel, maximum torque per copper losses (MTPCL), nonlinear controller.**

NOMENCLATURE

$\vec{V}, \vec{I}, \vec{\psi}$	Voltage, current, flux vectors
T_e	Electromagnetic torque
$\boldsymbol{R}$	Winding resistance
$\boldsymbol{L}$	Inductance
$\boldsymbol{L_l}$	Leakage inductance
L_{1r}, L_{2r}	Coupling inductances between the stator windings and the rotor
$\boldsymbol{p}$	Pole pair number
$\boldsymbol{N_r}$	Number of nests
ω_1, ω_2	Angular speed
$\boldsymbol{s}$	Slip
θ	Current angle
$\boldsymbol{f}$	Frequency
$\boldsymbol{X}$	Vector of the state variables
$\boldsymbol{F}, \boldsymbol{G}$	Nonlinear functions
$\boldsymbol{U}, \boldsymbol{Y}$	Vectors of input and output
$\boldsymbol{P}, \boldsymbol{Q}$	Nonlinear functions in the output error dynamic
$\boldsymbol{\eta}$	Vector of output error
$\boldsymbol{S}$	Positive-semi definite storage function
$\boldsymbol{E}$	Output tracking error
Δ	Vector of system uncertainties
$\hat{\Delta}$	Estimation of Δ
$\boldsymbol{\varepsilon}$	Estimation error
$\boldsymbol{\rho}$	Upper bound of the estimation error
$\boldsymbol{\mu}$, $\boldsymbol{\Gamma}$	Positive diagonal matrixes
$\boldsymbol{z}, \boldsymbol{Z}$	Positive constant
$\boldsymbol{v}$	New control input designed with the passivity concept
$\boldsymbol{M}$	Constant matrix
$\boldsymbol{\gamma_1}, \boldsymbol{\gamma_2}, \boldsymbol{\gamma_3}$	Constant values
$\boldsymbol{Im}[.]$	Imaginary part

Subscripts

$\boldsymbol{1}, \boldsymbol{2}, \boldsymbol{r}$	PW, CW and rotor
$\boldsymbol{d}, \boldsymbol{q}$	Rotating frame axis
$\boldsymbol{\alpha}, \boldsymbol{\beta}$	Stationary frame axis

I. INTRODUCTION

THE recent development in the field of doubly-fed electrical machines have attracted significant research interest due to their unique structure where only a partially rated power electronic converter is required, leading to a lower converter cost and lower power losses [1]. A doubly-fed electrical machine have two sets of three-phase windings, transferring electrical power between the machine and the power grid. The brushless doubly-fed induction machine (BDFIM) belongs to this family of machines, which has been close to commercialization in recent years, as both generators and variable speed drives. A BDFIM has some outstanding features of both squirrel cage induction machines and conventional synchronous machines. Other features of a BDFIM include: 1) precise synchronous operation over a wide speed range by the frequency control of the control winding (CW), 2) brushless structure, and 3) fault tolerant operation during converter failures. However, its special rotor structure, its stator with two isolated windings, and the relatively complex equivalent circuit are major bottlenecks in developing the BDFIM's concept.

This work was supported in part by Natural Science and Engineering Research Council of Canada (NSERC) Discovery Grant RGPIN-2016-04170 (*Corresponding author: Xiaodong Liang*).

Hamidreza Mosaddegh Hesar and Xiaodong Liang are with the Department of Electrical and Computer Engineering, University of Saskatchewan, Saskatoon, SK, S7N 5A9, Canada (e-mail: pvt356@usask.ca, xil659@mail.usask.ca).

Hossein Abootorabi Zarchi and Amir Khazaee are with the Department of Electrical Engineering, Faculty of Engineering, Ferdowsi University of Mashhad, Mashhad, 9177948974, Iran (e-mail: abootorabi@um.ac.ir, amir.khazaee@alumni.um.ac.ir).

Hamed Chenarani is with the Department of Electrical Engineering, Shahrood University of Technology, Shahrood, 3619995161, Iran (e-mail: hamed.chenarani@shahroodut.ac.ir).

In this regard, the research carried out on BDFIMs can be mostly categorized into two major scopes: 1) optimizing the machine's design process [2]-[5], and 2) developing effective control techniques considering the doubly-fed structure [6]-[9]. In the second scope, conventional control structures can be augmented by adding a control strategy, such as the maximum torque per copper losses (MTPCL) control, which significantly increases the potential of a BDFIM drive in industrial applications. The main issue of a BDFIM is the presence of an uncontrollable power winding (PW). Singly-fed machines are fully controllable and the MTPCL can be easily implemented for them; while there exists a serious challenge to implement the MTPCL for a BDFIM in which only the CW is controllable.

Increasing the efficiency of the entire drive system is always desired, and the MTPCL strategy is an intelligent solution to enhance the efficiency of the machine. Basically, the goal of the MTPCL strategy is to provide the torque with the lowest copper losses, which leads to an increased overall system efficiency since copper losses are usually larger than core losses and other losses [10]. In this regard, extensive research has been conducted on energy saving using the MTPCL-based control technique for singly-fed electric machines in [11]-[15].

Currently, only limited studies have been conducted in the field of control strategies for BDFIMs, such as the efficiency optimization and the MTPCL. Basically, this deficiency is present in the entire family of brushless doubly-fed machines, but it is more severe in BDFIMs. In [16], a simple search algorithm based on the microcontroller is introduced to maximize the efficiency of the BDFIM pump drive, which can be used to maximize the efficiency of any type of BDFIM variable speed drive. In this algorithm, by choosing the value of the CW's current, the input power of the machine is minimized under any speed and any loading conditions. An analytical method using a core model to maximize the torque-to-current ratio of a BDFIM under steady state is presented in [17]. To realize this strategy, the torque relationship in terms of one of the currents of PW and CW needs to be extracted, a unique current is defined for optimization, from which the optimal angle of the current corresponding to the maximum torque is obtained based upon the core model. Furthermore, by dividing the torque relationship into two synchronous and asynchronous torques, the effect of pole pairs of PW and CW on the maximum torque is investigated in this paper. In [18], Betz et al. introduce two control strategies for brushless doubly-fed reluctance machines (BDFRMs) based on the BDFRM model, the maximum torque per inverter ampere and the maximum torque per total ampere, these strategies are intended to be used in variable speed drives. Nevertheless, in their subsequent studies, only the performance of the first strategy has been investigated in the BDFRM drive [19]-[21]. In [22], the maximum torque per total ampere strategy based on the search method is presented for the BDFIM drive, where the total stator current is minimized for a given load torque by a stepwise change of the CW's direct (d)-axis current.

According to the authors' best knowledge, the MTPCL control strategy has not yet been proposed for BDFIMs in the literature. In this paper, a novel control structure by combining a nonlinear controller and an online optimization algorithm based on the control of the CW current's angel is introduced for the BDFIM drive. The target of this strategy is to deliver the electromagnetic torque with the minimized copper loss to achieve an improved overall system efficiency. The main contribution and novelty of the paper include:

- A theoretical approach is proposed to realize a model-based MTPCL control as one of the most important control property of BDFIMs. Due to the flux and frame alignment conditions, current angles of PW and CW are not independent. In this regard, a fundamental relationship is obtained between the two angles, and the expression of copper losses in terms of the angle of the CW's current can thus be derived. The optimal angle, which realizes the control strategy, is then calculated by using a numerical minimization procedure.
- The presence of nonlinear dynamics in BDFIMs demands new nonlinear control techniques. In this paper, a robust adaptive nonlinear controller is developed based on the passivation method. The passivation method uses the passivity concept and ensures the global asymptotic stability of a closed-loop system, and thus, is suitable for the controller design with a simple control law for complex nonlinear systems [23],[24],[25]. A nonlinear feedback law is designed based on the passivity concept to form a passive closed-loop system for BDFIMs. The Taylor series expansion is utilized to estimate uncertain terms with the aid of simple adaptation laws.

This controller preserves all benefits of model-based control approaches, such as fast response and high accuracy. It converges within a certain tolerance of the optimum without perturbations that affect the steady-state system performance. The dependency of the proposed strategy on machine parameters is also solved using the robust nonlinear controller. The proposed control structure is suitable for applications that require very fast update of control variables, e.g., electric vehicles and hybrid electric vehicles.

The rest of paper is organized as follows: In Section II, the reduced-order model of BDFIMs is introduced. Section III presents the principle of the proposed MTPCL control strategy and how to obtain its realization criterion. The design of the nonlinear controller with an emphasis on the concept of passivity is proposed in Section IV. In Section V, the experimental results are presented and analyzed. Section VI contains the concluding remarks.

II. Basic Principle, Structure and Model of BDFIMs

A. The Basic Principle and Structure of BDFIMs

The BDFIM is a single-frame brushless induction machine with two balanced three-phase windings placed on its stator. Although it is possible to arrange one winding on the stator in such a way that it produces two different fields, it is preferable to have two isolated three-phase windings because in this case, the overall performance is better and the windings can also have

different capacities based on the needs. One of the two stator windings is the PW, which is directly connected to the grid and has a fixed frequency of the grid. Most of the power exchange between the grid and the machine is done by the PW. Another stator winding, known as the CW, is connected to the grid through a back-to-back converter with a capacity lower than the capacity of the machine. To prevent direct magnetic coupling between PW and CW, the number of pole pairs of the two windings must be different [26]. Also, to reduce the unbalanced magnetic pull on the rotor, the difference between the pole pairs must be greater than one [27].

B. The Model of BDFIMs

The two-axis dynamic fifth-order model of BDFIMs is written as follows [28]

$$\vec{V}_1 = R_1\vec{I}_1 + \frac{d\vec{\psi}_1}{dt} + j\omega_1\vec{\psi}_1 \tag{1}$$

$$\vec{V}_2 = R_2\vec{I}_2 + \frac{d\vec{\psi}_2}{dt} + j\omega_2\vec{\psi}_2 \tag{2}$$

$$\vec{\psi}_1 = L_1\vec{I}_1 + L_{12}\vec{I}_2^* \tag{3}$$

$$\vec{\psi}_2 = L_2\vec{I}_2 + L_{12}\vec{I}_1^* \tag{4}$$

where

$$L_1 = L_{12} + L_{l1} + \frac{L_{1r}.L_{lr}}{L_{1r}+L_{2r}+L_{lr}}$$

$$L_2 = L_{12} + L_{l2} + \frac{L_{2r}.L_{lr}}{L_{1r}+L_{2r}+L_{lr}}$$

$$L_{12} = -\frac{L_{1r}.L_{2r}}{L_{1r}+L_{2r}+L_{lr}}$$

In deriving the two-axis voltage equations, Eqs. (1) and (2) have been referred to the reference frames rotating at the angular speeds of PW and CW, ω_1 and ω_2, respectively [29]. The electromagnetic torque of the fifth-order model can be expressed by

$$T_e = -\frac{3}{2}N_r.L_{12}\,Im[\vec{I}_1^*\vec{I}_2^*] \tag{5}$$

III. The Proposed Maximum Torque per Copper Losses Control Strategy

A desirable strategy for controlling the BDFIM is to achieve the MTPCL control. In this strategy, it is necessary to derive the expression for the total copper losses based on angles of the PW and CW's currents. We have demonstrated below how this equation is derived.

The basic expression of the torque in (5) can be manipulated into a variety of forms. One form is

$$T_e = \gamma_1(\psi_{1d}i_{2q} + \psi_{1q}i_{2d}) \tag{6}$$

where $\gamma_1 = \frac{3}{2}\left(\frac{N_rL_{12}}{L_p}\right)$.

Another form of the torque is stated in terms of the two-axis components of the flux and the current of the PW as follows:

$$T_e = \gamma_2.(\psi_{1d}i_{1q} - \psi_{1q}i_{1d}) \tag{7}$$

where $\gamma_2 = \frac{3}{2}N_r$.

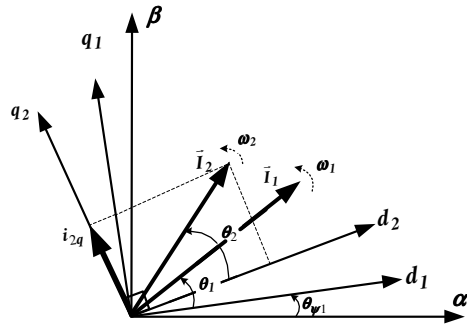

Fig. 1. Current vectors used in the equations and their inter-relationships.

The PW's flux orientation is achieved by aligning the d-axis of the synchronous reference frame with the PW's flux vector. Therefore, Eqs. (6) and (7) can be rewritten by

$$T_e = \gamma_1(|\vec{\psi}_1|i_{2q}) \tag{8}$$

$$T_e = \gamma_2(|\vec{\psi}_1|i_{1q}) \tag{9}$$

Therefore, the torque can be controlled by the quadrature (q)-axis current of the PW and CW, respectively. From Fig. 1, it can be observed that

$$T_e = \gamma_1|\vec{\psi}_1||\vec{I}_2|\sin\theta_2 \tag{10}$$

$$T_e = \gamma_2|\vec{\psi}_1|.|\vec{I}_1|\sin\theta_1 \tag{11}$$

Substituting $\vec{I}_1 = |\vec{I}_1|e^{j\theta_1}$ and $\vec{I}_2 = |\vec{I}_2|e^{j\theta_2}$ into (5), the following equation can be derived after a few manipulations:

$$T_e = \gamma_3|\vec{I}_1|.|\vec{I}_2|\sin(\theta_1+\theta_2) \tag{12}$$

where $\gamma_3 = \gamma_2L_{12}$.

Comparing (10) and (12), the PW's current magnitude can be obtained as follows:

$$|\vec{I}_1| = \frac{|\vec{\psi}_1|\sin\theta_2}{L_p\sin(\theta_1+\theta_2)} \tag{13}$$

Similarly, for the CW's current magnitude, we have

$$|\vec{I}_2| = \frac{|\vec{\psi}_1|\sin\theta_1}{L_{12}\sin(\theta_1+\theta_2)} \tag{14}$$

The copper losses of BDFIMs can be expressed by

$$\begin{aligned} P_{cu} &= R_1|\vec{I}_1|^2 + R_2|\vec{I}_2|^2 \\ &= R_1\left(\frac{|\vec{\psi}_1|\sin\theta_2}{L_p\sin(\theta_1+\theta_2)}\right)^2 + R_2\left(\frac{|\vec{\psi}_1|\sin\theta_1}{L_{12}\sin(\theta_1+\theta_2)}\right)^2 \\ &= \frac{R_1|\vec{\psi}_1|^2L_{12}^2(\tan\theta_2)^2}{(\cos\theta_1)^2} + \frac{R_2|\vec{\psi}_1|^2L_p^2(\tan\theta_1)^2}{(\cos\theta_2)^2} \\ &= \frac{}{L_p^2L_{12}^2(\tan\theta_1+\tan\theta_2)^2} \end{aligned} \tag{15}$$

To minimize (15) for a given torque, it is necessary to find an axillary relationship between angles of the PW and CW's currents, θ_1 and θ_2, respectively. Using (3) and (9), we have

$$\frac{i_{2q}}{i_{2d}} = \tan\theta_2 = \frac{T_eL_p}{\gamma_2|\vec{\psi}_1|(|\vec{\psi}_1| - L_pi_{1d})} \tag{16}$$

This expression can be simplified to give

This article has been accepted for publication in IEEE Transactions on Energy Conversion. This is the author's version which has not been fully edited and content may change prior to final publication. Citation information: DOI 10.1109/TEC.2022.3224637

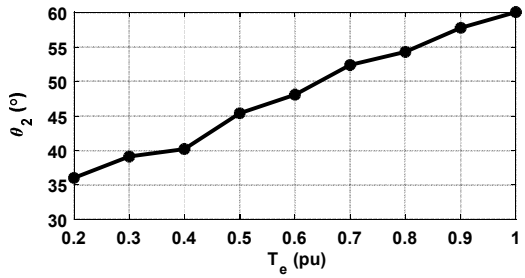

Fig. 2. The CW's current Angles (θ_2) under the MTPCL Control.

$$i_{1d} = \frac{\gamma_2 |\vec{\psi}_1|^2 \tan\theta_2 - T_e L_p}{\gamma_2 |\vec{\psi}_1| L_p \tan\theta_2} \tag{17}$$

Likewise, from (9) and (17), we have

$$\frac{i_{1q}}{i_{1d}} = \tan\theta_1 = \frac{T_e L_p \tan\theta_2}{\gamma_2 |\vec{\psi}_1|^2 \tan\theta_2 - T_e L_p} \tag{18}$$

Eq. (18) is a fundamental relationship that exists between angles of the PW and CW's currents, and it is useful to express copper losses in terms of θ_2, as a controllable variable. By knowing $cos\theta_i = 1/\left(\sqrt{1+tan^2\theta_i}\right), (i = 1,2)$ and substituting (18) into (15), an expression is achieved for P_{cu} in terms of θ_2 in (19). In practice, the derivative of this expression with respect to $\tan\theta_2$ is complicated and cannot be solved analytically. Hence, the optimal angles are determined using a numerical minimization procedure implemented in MATLAB.

Fig. 2 shows the CW's current angles under the MTPCL control. To realize this control, the relationship between d- and q-axis components of the CW's current is determined by

$$\tan\theta_2 = i_{2q}/i_{2d} \Rightarrow i_{2d}\tan\theta_2 - i_{2q} = 0 \tag{20}$$

According to (20), the MTPCL control strategy is realized when $i_{2d}tan\theta_2 - i_{2q}$ tracks zero as command.

IV. Nonlinear Controller Design

A. Basic Concept of Passivity

Considering the following nonlinear affine system,

$$\dot{X} = F(X) + G(X)u \tag{21}$$

where $x \in R^n$ is the state vector, $u \in R^m$ is the input vector, and $y \in R^m$ is the output vector of the system. Also, the nonlinear continuous vector function $f(x): R^n \longrightarrow R^n$ and the matrix function $g(x): R^n \longrightarrow R^{n\times m}$ are locally Lipschitz, and $h(x): R^n \longrightarrow R^m$ is a continuous vector function ($f(0) = h(0) = 0$).

Definition 1 [30]*:* The system expressed in (21) is passive, between the input *u* and the output *y*, if there exists a positive semi-definite function $S: R^n \longrightarrow R$ (S(0)=0), such that,

$$\dot{S} \le y^T u \tag{22}$$

This function is the storage function.

Definition 2 [30]: If the condition of the passivity property changes as

$$\dot{S} \le y^T u - Zy^2 \tag{23}$$

Then, the system in (21) is output strictly passive (OSP) between the input *u* and the output *y*.

Definition 3 [30]*:* The system in (21) is zero-state observable (ZSO), if there is no solution of $\dot{X} = F(x) + G(x)U$ with $U \equiv 0$, which satisfies$\{h(x) = 0\}$, except the solution $x(t) \equiv 0$.

Lemma1 [30]*:* The unforced system (U = 0) in (21) is asymptotically stable, if it is OSP and ZSO.

To obtain the control inputs, the nonlinear control technique is applied to the BDFIM drive system. Therefore, by choosing $x_1 = i_{1d}, x_2 = i_{1q}, x_3 = i_{2d}, x_4 = i_{2q}$ and $x_5 = \omega_r$ as the state variables, $Y = [y_1 \;\; y_2]^T$ as the output vector, and $U = [u_1 \;\; u_2]^T$ as the input vector, the fifth-order affine model is described by (21), with $X = [x_1 \; x_2 \; x_3 \; x_4 \; x_5]^T = \left[i_{1d} \; i_{1q} \; i_{2d} \; i_{2q} \; \omega_r\right]^T$, the equation shown at the top of next page, and

$$G(X) = [g_1 \;\; g_2] = \frac{1}{\sigma . L_{12}} . \begin{bmatrix} 1 & 0 & -\frac{L_p}{L_{12}} & 0 & 0 \\ 0 & -1 & 0 & -\frac{L_p}{L_{12}} & 0 \end{bmatrix}^T$$

where $\sigma = 1 - (L_p . L_s / L_{12}^2)$ and $T_e = \frac{3}{2} N_r . L_{12} . (x_1 . x_4 + x_2 . x_3)$.

B. Robust Controller Design

Choosing the MTPCL strategy in (20) and the BDFIM torque as the output variables, tracking errors are introduced by

$$E = \begin{bmatrix} e_{y_1} \\ e_{y_2} \end{bmatrix} = \begin{bmatrix} y_1 - y_{1_{ref}} \\ y_2 - y_{2_{ref}} \end{bmatrix} = \begin{bmatrix} i_{2d}\tan\theta_2 - i_{2q} \\ T_e - T_{e,ref} \end{bmatrix} \tag{24}$$

The error dynamics for the desirable output tracking purpose is defined as follows

$$\dot{E} = P + QU + \Delta \tag{25}$$

where the parameters are defined as shown at the bottom of the next page.

$$P_{cu} = \frac{R_1|\psi_1|^2 L_{12}^2 \tan^2\theta_2 + \left(\frac{T_e L_p \tan\theta_2}{\gamma_2|\vec{\psi}_1|^2 \tan\theta_2 - T_e L_p}\right)^2 \left(R_2|\psi_1|^2 L_p^2 + \left(R_1|\psi_1|^2 L_{12}^2 + R_2|\psi_1|^2 L_p^2\right)\tan^2\theta_2\right)}{L_p^2 L_{12}^2 \left(\tan^2\theta_2 + \left(\frac{T_e L_p \tan\theta_2}{\gamma_2|\vec{\psi}_1|^2 \tan\theta_2 - T_e L_p}\right)^2 + \frac{2T_e L_p \tan^2\theta_2}{\gamma_2|\vec{\psi}_1|^2 \tan\theta_2 - T_e L_p}\right)} \tag{19}$$

$$F(X) = [f_1 \;\; f_2 \;\; f_3 \;\; f_4 \;\; f_5] = \begin{bmatrix} \frac{1}{\sigma . L_{12}}\left(-\frac{L_s}{L_{12}}V_{1d} + \frac{R_1 . L_s}{L_{12}} . x_1 + \omega_2 . (L_s . x_4 - L_{12} . x_2) - R_2 . x_3\right) \\ \frac{1}{\sigma . L_{12}}\left(-\frac{L_s}{L_{12}}V_{1q} + \frac{R_1 . L_s}{L_{12}} . x_2 + \omega_2 . (L_s . x_3 + L_{12} . x_1) + R_2 . x_4 + \frac{\omega_1 . L_s . |\vec{\psi}_1|}{L_{12}}\right) \\ \frac{1}{\sigma . L_{12}}\left(V_{1d} - R_1 . x_1 + \omega_2 . L_p . (x_2 - \frac{L_s}{L_{12}} . x_4) + \frac{R_2 . L_p}{L_{12}} . x_3\right) \\ \frac{1}{\sigma . L_{12}}\left(-V_{1q} + R_1 . x_2 + \omega_2 . L_p . (x_1 + \frac{L_s}{L_{12}} . x_3) + \frac{R_2 . L_p}{L_{12}} . x_4 + \omega_1 . |\vec{\psi}_1|\right) \\ \frac{1}{J}(T_e - T_L - B . x_5) \end{bmatrix}^T$$

The following adaptive control law ensures the asymptotic stability of (25)

$$U = Q^{-1}\left[-P - \hat{\Delta} - \Gamma E + v\right] \tag{26}$$

In this way, the first order Taylor series expansion is utilized to approximate Δ. Therefore, consider $\hat{\Delta}$ as follows:

$$\begin{aligned} \hat{\Delta} &= \hat{Z}_0 + \frac{\partial \hat{\Delta}}{\partial E}|(0,0)E + \frac{\partial \hat{\Delta}}{\partial \dot{E}}\Big|(0,0)\dot{E} \\ &= \hat{Z}_0 + \hat{Z}_1 E + \hat{Z}_2 \dot{E} \end{aligned} \tag{27}$$

For the simplicity, $\hat{\Delta}$ is represented by

$$\hat{\Delta} = \hat{M}^T \eta \tag{28}$$

where $\eta = [1 \quad E \quad \dot{E}]^T$ and $\hat{M}^T = [\hat{Z}_0 \quad \hat{Z}_1 \quad \hat{Z}_2]$. According to the BDFIM model, suppose that Δ can be modelled by

$$\Delta = M^T \eta + \varepsilon \tag{29}$$

By replacing the controller of (26) in (25), the closed-loop error dynamics will be

$$\dot{E} + \Gamma E = \Delta - \hat{\Delta} + v \tag{30}$$

Moreover, using (28) and (29), we have

$$\dot{E} + \Gamma E = \left(M^T - \hat{M}^T\right)\eta + \varepsilon + v \tag{31}$$

If the uncertainty term Δ is approximated by the first Taylor series expansion, then we have

$$\left|\Delta - \hat{\Delta}\right| < z \tag{32}$$

Suppose that

$$\left|\Delta - \hat{M}^T \eta\right| < \rho \tag{33}$$

Therefore, $|\varepsilon| < \rho$, in which ρ is the upper bound of the error estimation.

C. The Stability Proof

The following positive definite function is suggested to obtain the adaptive laws:

$$V = \frac{1}{2}E^T E + \frac{1}{2}\left(\hat{M} - \hat{M}^T\right)^T \mu \left(\hat{M} - \hat{M}^T\right) \tag{34}$$

The time derivative of V is expressed by

$$P = \begin{bmatrix} p_1 \\ p_2 \end{bmatrix} = \begin{bmatrix} \frac{tg\theta_2}{\sigma L_{12}}\left(-\left(\frac{L_s}{L_{12}}x_4\right)\omega_2 L_p + \frac{R_2 L_p}{L_{12}}x_3\right) - \frac{1}{\sigma L_{12}}\left[\frac{\omega_2 L_p L_s}{L_{12}}x_3 + \frac{R_2 L_p}{L_{12}}x_4\right] \\ \frac{3}{2}N_r L_{12}\left[\frac{x_4}{\sigma L_{12}}\left(-\frac{L_s}{L_{12}}V_{1d} + \omega_2 L_s x_4 - R_2 x_3\right)\right] + \frac{3}{2}N_r L_{12}\left[\frac{x_3}{\sigma L_{12}}\left(-\frac{L_s}{L_{12}}V_{1q} + \omega_2 L_s x_3 + R_2 x_4\right)\right] \end{bmatrix}$$

$$Q = \begin{bmatrix} q_{11} & q_{12} \\ q_{21} & q_{22} \end{bmatrix} = \begin{bmatrix} -\frac{tg\theta_2}{\sigma L_{12}} & \frac{L_p}{L_{12}} \\ \frac{3}{2}N_r L_{12} x_4 & -\frac{3}{2}N_r L_{12} x_3 \end{bmatrix}$$

$$\Delta = \begin{bmatrix} \Delta_1 \\ \Delta_2 \end{bmatrix} = \begin{bmatrix} \frac{tg\theta_2}{\sigma L_{12}}\left(V_{1d} - R_1 x_1 + \omega_2 L_p x_2\right) - \frac{1}{\sigma L_{12}}\left[-V_{1q} + R_1 x_2 + \omega_2 L_p x_1 + \omega_1 |\vec{\lambda_1}|\right] \\ \frac{3}{2}N_r L_{12}\left[\begin{array}{l} \frac{x_4}{\sigma L_{12}}\left(\frac{R_1 L_s}{L_{12}}x_1 - \omega_2 L_{12} x_2\right) + \frac{x_1}{\sigma L_{12}}\left[-V_{1q} + R_1 x_2 + \omega_2 L_p\left(x_1 + \frac{L_s}{L_{12}}x_3\right)\right. \\ \left. + \frac{R_2 L_p}{L_{12}}x_4 + \omega_1 |\vec{\lambda_1}|\right] - \frac{L_p}{L_{12}}u_2 x_1 + \frac{x_2}{\sigma L_{12}}\left(V_{1d} - R_1 x_1 + \omega_2 L_p\left(x_2 - \frac{L_s}{L_{12}}x_4\right)\right. \\ \left. + \frac{R_2 L_p}{L_{12}}x_3\right) - \frac{L_p}{L_{12}}u_1 x_2 \end{array}\right] \end{bmatrix}$$

This article has been accepted for publication in IEEE Transactions on Energy Conversion. This is the author's version which has not been fully edited and content may change prior to final publication. Citation information: DOI 10.1109/TEC.2022.3224637

$$\begin{aligned}\dot{V} &= E^T\dot{E} - \left(M^T - \hat{M}^T\right)^T \mu\dot{\hat{M}}^T \\ &= E^T\left[-\Gamma E + \left(M^T - \hat{M}^T\right)\eta + \varepsilon + v\right] - \left(M^T - \hat{M}^T\right)^T \mu\dot{\hat{M}}^T \\ &= -E^T\Gamma E + E^T\varepsilon + E^T v + \left(M^T - \hat{M}^T\right)^T\left(\eta^T E - \mu\dot{\hat{M}}^T\right)\end{aligned} \tag{35}$$

If $\eta^T E - \mu\dot{\hat{M}}^T = 0$, the adaptive law is:

$$\dot{\hat{M}} = E^T\eta(\mu^{-1})^T \tag{36}$$

Therefore, Eq. (35) can be rewritten as (37).

$$\dot{V} = -E^T\Gamma E + E^T\varepsilon + E^T v \tag{37}$$

According to Lemma 1, if $E^T\varepsilon < E^T\Gamma E$, then the closed-loop system in (30) is OSP between the output error E and the new control input v. Also, this closed-loop system is ZSO in accordance with Definition 3. Therefore, the asymptotic stability of the error dynamics in (25) is guaranteed with $v = 0$. With the usage of Cauchy–Schwartz inequality and by considering $|\varepsilon| < \rho$, we have

$$E^T\varepsilon \le \|E\|.|\varepsilon| < \|E\|.\rho \tag{38}$$

On the other hand,

$$\lambda_{min}(\Gamma)\|E\|^2 \le E^T\Gamma E < \lambda_{max}(\Gamma)\|E\|^2 \tag{39}$$

Thus, the following condition should be satisfied for $E^T\varepsilon < E^T\Gamma E$:

$$\|E\|.\rho < \lambda_{min}(\Gamma).\|E\|^2 \rightarrow r \overset{\Delta}{=} \frac{\rho}{\lambda_{min}(\Gamma)} < \|E\| \tag{40}$$

In other words, the norm of the error is uniformly bounded in a circle region with the radius of r. It is worth noting that the norm of the error and its upper derivatives depend on the upper bound of the approximation ρ, and also, Γ. The higher gain values make the amplitude of the error smaller. However, a compromise must be made between them.

V. Results and Discussions

The experimental setup shown in Fig. 3 consists of a BDFIM coupled to a DC generator, a 1024 incremental encoder and the control drive system hardware. The control drive system hardware is composed of six parts: an IGBT-based three-phase inverter with six gate drivers independently to power the motor; voltage and current sensors; an analog filter; a digital signal processor (DSP) TMS320F28335; and a emulator. The stator's phase currents are measured by Hall-effect current sensors (LEM LTS-6-NP). Table I shows the specifications of a 3 kW prototype D132s-BDFIM (D132 is the frame size).

TABLE I
Parameters of the D132 BDFIM Prototype Used in Experiments

Symbol	Value	Symbol	Value
p_1/p_2	2/4	R_r	1.1237 (Ω)
I_1	10 (A)	L_{1r}	0.1863 (H)
I_2	4.5 (A)	L_{2r}	0.0998 (H)
T_e	20 (N.m)	L_{l1}	0.0047 (H)
R_1	1.3012 (Ω)	L_{l2}	0.0053 (H)
R_2	3.7171 (Ω)	L_{lr}	0.0206 (H)

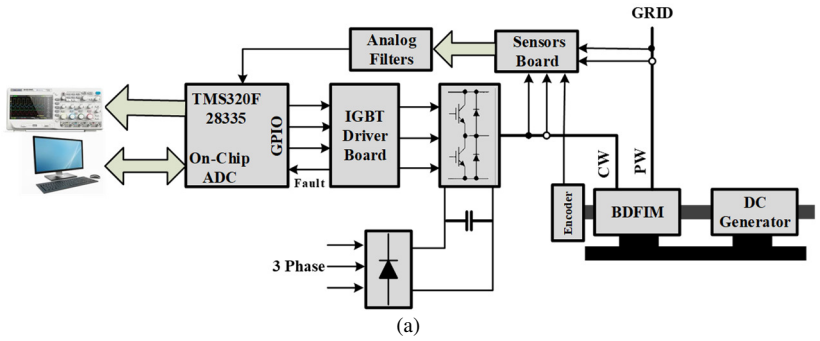

(a)

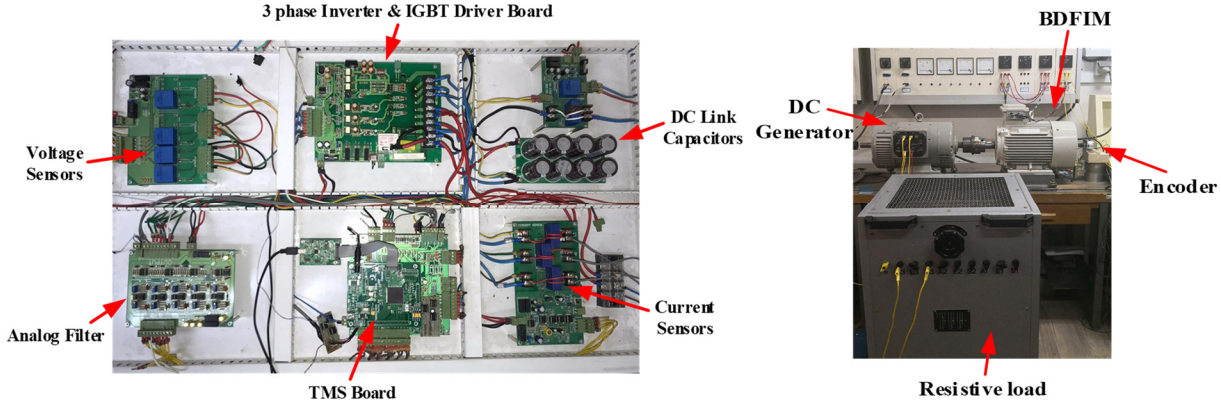

(b)

Fig. 3. Experimental setup: (a) the implementation block diagram, and (b) the BDFIM drive hardware.

This article has been accepted for publication in IEEE Transactions on Energy Conversion. This is the author's version which has not been fully edited and content may change prior to final publication. Citation information: DOI 10.1109/TEC.2022.3224637

The performance of the proposed MTPCL control strategy is analyzed based on experimental results. The block diagram of the proposed MTPCL control is shown in Fig. 4. In this regard, the torque command changes periodically between 0.5 pu and 1 pu. As observed in Figs. 5a and 5b, the proposed nonlinear controller is capable of achieving both control objectives: 1) minimization of copper losses, and 2) high dynamic torque regulation.

As indicated in (20), the MTPCL control will be satisfied when its realization criterion tracks zero as the reference value. Changes in their current magnitudes in PW and CW are illustrated in Figs. 5c, and 5d, based on the pattern of the torque reference. Although the PW's current magnitude is relatively constant with variations of the torque, the CW's current magnitude changes significantly with variations of the torque. The reason can be explained through (10). Eq. (10) is a function of the magnitude and angle of the CW's current. Since angle changes in the CW's current are not large as the torque increases (Fig. 1), the magnitude of the CW's current must increase considerably to follow the torque reference.

Fig. 6 shows waveforms obtained during the motor start-up with a torque's step reference variation, from zero to 0.5 pu. According to this figure, the proposed nonlinear controller results in a fast dynamic response with a better rise time compared to the conventional proportional-integral (PI) controller. This comparison is also done in the dynamic test (similar to Fig. 5) for the MTPCL control criterion. As illustrated in Fig. 7, the performance of the linear PI controller to track the reference value is relatively poor, especially during transients. To quantify results of Figs. 5a and 7, two performance indices, including the integral absolute error (IAE), and the integral time-weighted absolute error (ITAE), are investigated. IAE integrates the absolute error over time and ITAE integrates the absolute error multiplied by the time over time. Smaller values of IAE and ITAE indicate that the proposed controller performs better in tracking the reference signal. The results show that IAE (ITAE) are equal to 0.0198 (0.0183) for the proposed controller, and 0.0231 (0.0257) for the PI controller, which is almost 116 % (140 %).

To further study the proposed strategy, the performance of the MTPCL strategy is investigated with the closed-loop speed control. In this experimental test, the speed error is delivered to the PI controller, and the torque command is then achieved from the controller output. Under this condition, the load torque is stepped up from 0.4 to 0.6 pu at the fixed rotor speed. Fig. 8 shows copper losses of the BDFIM with and without the proposed MTPCL control strategy. It can be seen that under the MTPCL control, P_{cu} reduces compared to the constant flux method. To achieve the conventional FOC, the flux control loop is substituted with the control loop of the MTPCL strategy. Therefore, the CW flux command is set on its nominal value.

The estimation error of the adaptive approach is presented in Fig. 9 during the transient of the motor start-up. The uncertainty terms Δ_1 and Δ_2 are considered as unknown functions and only their outputs are measurable. This figure shows $|\Delta_1 - \hat{\Delta}_1|$ and $|\Delta_2 - \hat{\Delta}_2|$. We can see that the error converges to zero and stay in an acceptable band. This confirms the capability of the adaptive Taylor-series expansion.

The efficiency improvement of the BDFIM drive using the proposed MTPCL control compared to the rated flux strategy is illustrated in Table II through experiments in the lab, for the

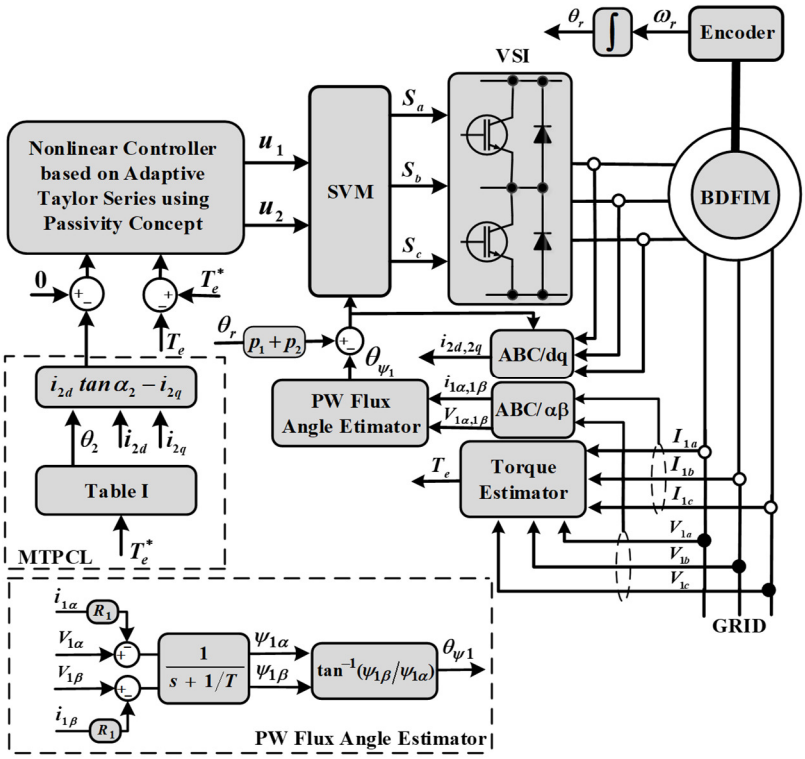

Fig. 4. The block diagram of the BDFIM drive system.

This article has been accepted for publication in IEEE Transactions on Energy Conversion. This is the author's version which has not been fully edited and content may change prior to final publication. Citation information: DOI 10.1109/TEC.2022.3224637

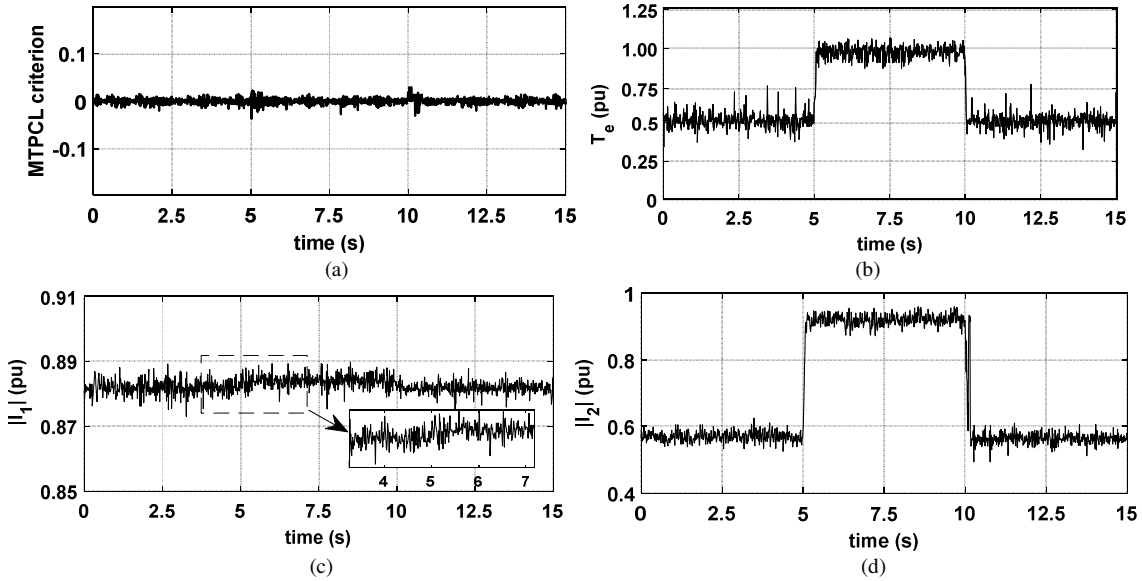

Fig. 5. The dynamic performance of the proposed control strategy: (a) MTPCL realization criterion; (b) Electromagnetic torque; (c) PW current magnitude; (d) CW current magnitude.

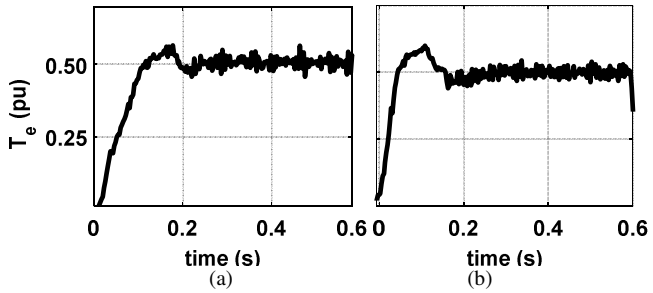

Fig. 6. Electromagnetic torque during the torque step variation from 0 to 0.5pu: (a) PI controller, (b) proposed nonlinear controller.

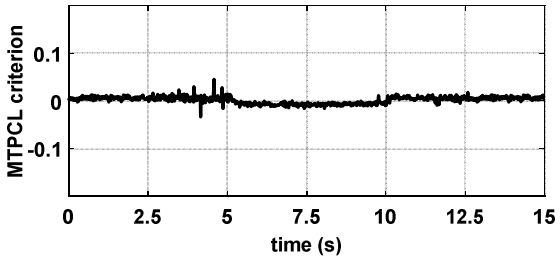

Fig. 7. The performance of the PI controller when tracking the zero command.

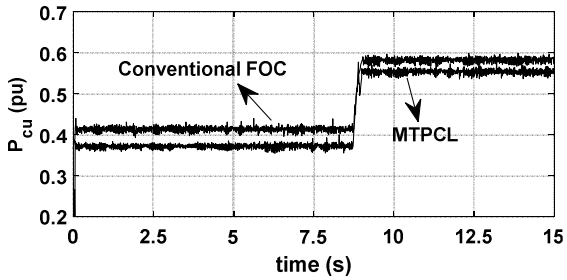

Fig. 8. Copper losses with and without the MTPCL control.

Table II
A BDFIM's Efficiency Improvement (Experimental Results)

	$T_l = 0.4\ pu$	$0.6\ pu$	$0.8\ pu$	$1\ pu$
$n_r = 0.8\ pu$	3.03%	2.11%	1.17%	Negligible
$n_r = 1.2\ pu$	3.41%	2.32%	1.41%	Negligible

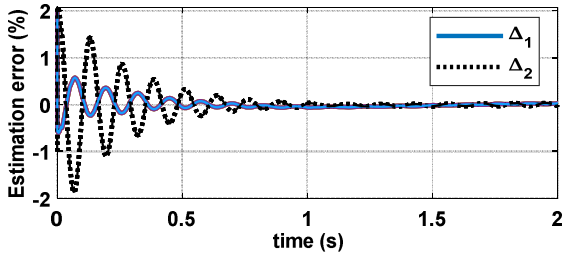

Fig. 9. The estimation error of the proposed adaptive approach.

Table III
The CW's Power Factors Under the MTPCL Control

	Torque (pu)								
	0.2	0.3	0.4	0.5	0.6	0.7	0.8	0.9	1
PF	0.52	0.55	0.58	0.60	0.62	0.66	0.67	0.68	0.71

rotor speed equal to 0.8 and 1.2 p.u, and the load torque equal to 0.4, 0.6, 0.8, and 1 p.u. It shows that a higher improvement of efficiency is achieved at a smaller load. Power factors of the CW obtained by experiments are also given in Table III in the operating range of BDFIMs under the MTPCL control.

It is obvious that Eq. (19) is dependent on having knowledge of L_{12} and L_{p}. Since L_{12} and L_{p} are affected by saturation level of the machine, the question arises as to how accurately these parameters must be known. To determine this, a sensitivity analysis is carried out to determine the effect that inaccurate knowledge of L_{12} and L_{p} has on P_{cu} under the MTPCL control. The results are plotted in Figs. 10a and 10b. It is found that although the minimum value of P_{cu} is relatively sensitive to L_{12}, it is insensitive to an error in L_p when it is in the range of ±50%. It is worth noting that Eq. (19) is not dependent on the rotor speed and the frequency, since the PW is directly connected to the power grid, and the frequency of its voltage and current is governed by the grid and considered fixed.

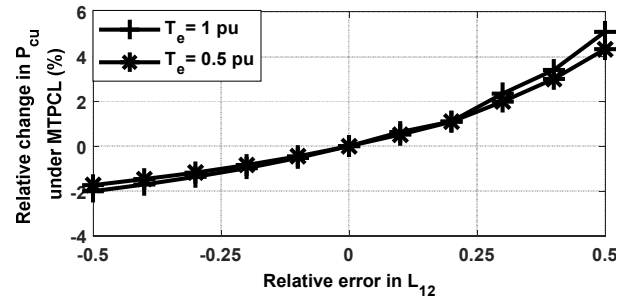

(a)

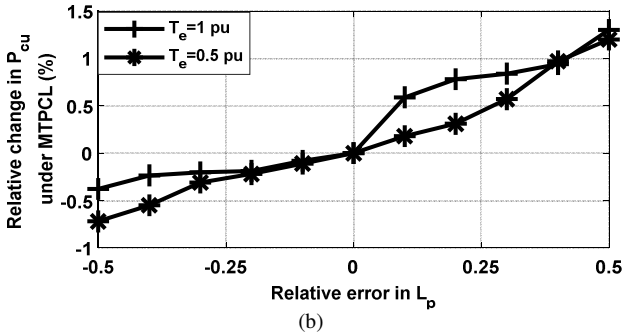

(b)

Fig. 10. Relative changes in copper losses vs. the error in: (a) L_{12}, and (b) L_p.

VI. Conclusion

A novel MTPCL control strategy is proposed in this paper for BDFIM drives on the basis of adaptive Taylor series to maximize the ratio of torque to copper losses. At the first glance, it seems that this strategy is not applicable due to the presence of uncontrollable PW. To leave this dead end, in this paper, the expression of copper losses was derived in terms of the angle of the CW's current with the aid of an axillary relationship. The minimization can be simplified to a one-variable minimization problem. Using this equation, the realization criterion of the MTPCL, which is the ratio of the orthogonal-axis current to the direct-axis current, can be obtained. It is shown that when the realization criterion of the strategy is forced to zero by the nonlinear controller, this ratio is adjusted to minimize copper losses. Experimental results confirm the effectiveness of the proposed control method.

References

[1]. J. Mohammadi, S. Vaez-Zadeh, S. Afsharnia and E. Daryabeigi, "A Combined Vector and Direct Power Control for DFIG-Based Wind Turbines," *IEEE Transactions on Sustainable Energy*, vol. 5, no. 3, pp. 767-775, July 2014.

[2]. S. Abdi, E. Abdi and R. McMahon, "A New Iron Loss Model for Brushless Doubly-Fed Machines With Hysteresis and Field Rotational Losses," *IEEE Transactions on Energy Conversion*, vol. 36, no. 4, pp. 3221-3230, Dec. 2021.

[3]. X. Chen, W. Pan, X. Wang and Y. Zhou, "Design of a Brushless Doubly Fed Generator with Simplified Three-phase Wound Rotor," *IEEE Transactions on Industrial Electronics*, 2022.

[4]. H. Gorginpour, H. Oraee and R. A. McMahon, "Electromagnetic-Thermal Design Optimization of the Brushless Doubly Fed Induction Generator," *IEEE Transactions on Industrial Electronics*, vol. 61, no. 4, pp. 1710-1721, April 2014.

[5]. S. Abdi, E. Abdi, A. Oraee and R. McMahon, "Optimization of Magnetic Circuit for Brushless Doubly Fed Machines," *IEEE Transactions on Energy Conversion*, vol. 30, no. 4, pp. 1611-1620, Dec. 2015.

[6]. M. G. Hussien, Y. Liu, W. Xu, A. K. Junejo and S. M. Allam, "Improved MRAS Rotor Position Observer Based on Control Winding Power Factor for Stand-Alone Brushless Doubly-Fed Induction Generators," *IEEE Transactions on Energy Conversion*, vol. 37, no. 1, pp. 707-717, March 2022.

[7]. H. Wang *et al*., "A Cascade PI-SMC Method for Matrix Converter-Fed BDFIM Drives," *IEEE Transactions on Transportation Electrification*, vol. 7, no. 4, pp. 2541-2550, Dec. 2021.

[8]. M. Bodson, "Speed Control for Doubly Fed Induction Motors With and Without Current Feedback," *IEEE Transactions on Control Systems Technology*, vol. 28, no. 3, pp. 898-907, May 2020.

[9]. J. Yang *et al*., "Sensorless Control of Brushless Doubly Fed Induction Machine Using a Control Winding Current MRAS Observer," *IEEE Transactions on Industrial Electronics*, vol. 66, no. 1, pp. 728-738, Jan. 2019.

[10]. S. Bolognani, L. Peretti, and M. Zigliotto, "On-line MTPA Control Strategy for DTC Synchronous Reluctance Motor Drives," *IEEE Transactions on Power Electronics*, vol. 26, no. 1, pp. 20-28, Jan. 2011.

[11]. V. P. Vujičić, "Minimization of Torque Ripple and Copper Losses in Switched Reluctance Drive," *IEEE Transactions on Power Electronics*, vol. 27, no. 1, pp. 388-399, Jan. 2012.

[12]. B. Asaei and B. Rahrovi, "Minimum-copper-loss control over full speed range of an IPMSM drive for hybrid electric vehicle application," *2010 IEEE Vehicle Power and Propulsion Conference*, pp. 1-6, 2010.

[13]. A. Khazaee, H. Abootorabi Zarchi, G. Arab Markadeh and H. Mosaddegh Hesar, "MTPA Strategy for Direct Torque Control of Brushless DC Motor Drive," *IEEE Transactions on Industrial Electronics*, vol. 68, no. 8, pp. 6692-6700, Aug. 2021.

[14]. A. G. Yepes, J. Doval-Gandoy and H. A. Toliyat, "Strategy With Smooth Transitions and Improved Torque–Speed Region and Stator Copper Loss for Two-Level Asymmetrical Six-Phase Induction Motor Drives Under Switch Faults," in *IEEE Transactions on Power Electronics*, vol. 36, no. 2, pp. 1954-1969, Feb. 2021.

[15]. Q. Zhang, J. Deng and N. Fu, "Minimum Copper Loss Direct Torque Control of Brushless DC Motor Drive in Electric and Hybrid Electric Vehicles," *IEEE Access*, vol. 7, pp. 113264-113271, 2019.

[16]. B. V. Gorti, G. C. Alexander, R. Spee and A. K. Wallace, "Microcontroller based efficiency-maximization for a brushless doubly-fed machine pump drive," *Proceedings of IEEE/IAS International Conference on Industrial Automation and Control*, pp. 377-381, 1995.

[17]. M. Ahmadian, B. Jandaghi and H. Oraee, "Maximum Torque per Ampere Operation of Brushless Doubly Fed Induction Machines," *Renew. Energies Power Qual. J.*, Vol.1, No.9, pp. 981-985, May 2011.

[18]. R. E. Betz and M. G. Jovanovic, "Theoretical analysis of control properties for the brushless doubly fed reluctance machine," *IEEE Transactions on Energy Conversion*, vol. 17, no. 3, pp. 332-339, Sep. 2002.

[19]. S. Ademi and M. Jovanović, "Maximum torque per inverter ampere control of brushless doubly-fed reluctance generators for wind turbines," *2014 International Symposium on Power Electronics, Electrical Drives, Automation and Motion*, pp. 883-888, 2014.

[20]. S. Ademi and M. G. Jovanović, "Vector Control Methods for Brushless Doubly Fed Reluctance Machines," *IEEE Transactions on Industrial Electronics*, vol. 62, no. 1, pp. 96-104, Jan. 2015.

[21]. S. Ademi, M. G. Jovanović, H. Chaal and W. Cao, "A New Sensorless Speed Control Scheme for Doubly Fed Reluctance Generators," *IEEE Transactions on Energy Conversion*, vol. 31, no. 3, pp. 993-1001, Sept. 2016.

[22]. H. Mosaddegh Hesar, H. Abootorabi Zarchi and G. Arab Markadeh, "Stator Flux Oriented Control of Brushless Doubly Fed Induction Motor Drives Based on Maximum Torque per Total Ampere Strategy," *2019 10th International Power Electronics, Drive Systems and Technologies Conference (PEDSTC)*, pp. 84-89, 2019.

[23]. H. Chenarani, and T. Binazadeh, "Passivity-Based Stability Analysis and Robust Practical Stabilization of Nonlinear Affine Systems with Non-vanishing Perturbations." *Journal of Electrical and Computer Engineering Innovations (JECEI)*, vol. 4, no. 1, pp. 39-47, Oct. 2016.

[24]. H. Chenarani, and M. Fateh, "Robust Passivity-based Sliding Mode Control of a Large Class of Nonlinear Systems Subject to Unmatched Uncertainties: A Robot Manipulator Case Study." *IETE Journal of Research*, vol. 68, no. 1, pp. 1-10, Sep. 2021.

[25]. M. M. Namazi, S. M. S. Nejad, A. Tabesh, A. Rashidi and M. Liserre, "Passivity-Based Control of Switched Reluctance-Based Wind System Supplying Constant Power Load," *IEEE Transactions on Industrial Electronics*, vol. 65, no. 12, pp. 9550-9560, Dec. 2018.

[26]. S. Williamson, A. C. Ferreira and A. Wallace, "Generalized Theory of the Brushless Doubly-Fed Machine-Part I: Analysis," *IEE Electric Power Application*, vol. 144, no. 2, pp. 111-122, Mar. 1997.

[27]. Ruqi Li, R. Spee, A. K. Wallace and G. C. Alexander, "Synchronous drive performance of brushless doubly-fed motors," *IEEE Transactions on Industry Applications*, vol. 30, no. 4, pp. 963-970, July-Aug. 1994.

[28]. S. Tohidi, "Analysis and Simplified Modelling of Brushless Doubly-Fed Induction Machine in Synchronous Mode of Operation", *IET Electric Power Applications,* vol. 10, no. 2, pp. 110-116, Feb. 2016.

[29]. R. E. Betz and M. G. Jovanovic, "Introduction to the Space Vector Modelling of the Brushless Doubly-Fed Reluctance Machine," *Electric Power Components and Systems*, vol. 31, no. 8, pp. 729–755, Jun. 2003.

[30]. H. K. Kahlil, *Nonlinear Control*, New York: Pearson, 2015.

Hamidreza Mosaddegh Hesar received the M.Sc. and Ph.D. degrees from Ferdowsi University of Mashhad, Iran, in 2014 and 2019, respectively, both in electrical engineering. He is currently working as a Postdoctoral Fellow at Power and Energy Conversion Laboratory, the University of Saskatchewan, Saskatoon, Canada. His research interests and activities include control of high-performance drives, modelling of electrical machines, and renewable energy.

Xiaodong Liang (M'06–SM'09) was born in Lingyuan, Liaoning, China. She received the B.Eng. and M.Eng. degrees from Shenyang Polytechnic University, Shenyang, China in 1992 and 1995, respectively, the M.Sc. degree from the University of Saskatchewan, Saskatoon, Canada in 2004, and the Ph.D. degree from the University of Alberta, Edmonton, Canada in 2013, all in electrical engineering.

From 1995 to 1999, she served as a lecturer at Northeastern University, Shenyang, China. In October 2001, she joined Schlumberger in Edmonton, Canada, and was promoted to a Principal Power Systems Engineer with this world's leading oil field service company in 2009. After working with Schlumberger for almost 12 years, from 2013 to 2019, she was with Washington State University in Vancouver, WA, United States and Memorial University of Newfoundland in St. John's, NL, Canada as an Assistant Professor and later an Associate Professor. In July 2019, she joined the University of Saskatchewan in Saskatoon, Canada, where she is currently an Associate Professor and Canada Research Chair in Technology Solutions for Energy Security in Remote, Northern, and Indigenous Communities. She was an Adjunct Professor with Memorial University of Newfoundland from 2019 to 2022. Her research interests include power systems, renewable energy, and electric machines.

Dr. Liang is a registered Professional Engineer in the province of Saskatchewan, Canada, a Fellow of IET, and a Deputy Editor-in-Chief of IEEE Transactions on Industry Applications.

Hossein Abootorabi Zarchi received the M.S. and Ph.D. degrees from Isfahan University of Technology, Isfahan, Iran in 2004 and 2010, respectively. From May 2009 to February 2010, he was a Visiting Ph.D. Student with the Control and Automation Group, Denmark Technical University, Denmark. He is currently an Assistant Professor at the Department of Electrical Engineering, Ferdowsi University of Mashhad, Mashhad, Iran. His research interests include electrical machines, nonlinear control of motor drives, and renewable energy.

Hamed Chenarani received his B.Sc. degree in communication engineering from Shahid Bahonar University of Kerman, Iran in 2012, his M.Sc. degree in control engineering from Shiraz University of Technology, Iran in 2014, and his Ph.D. Degree in electrical engineering from Shahrrod University of Technology, Iran in 2022. His research interests include robust nonlinear control, Passive Control, Robotics, and Intelligent Control. Currently, he is working on robust nonlinear control of Robot Manipulators.

Amir Khazaee received the M.Sc. degree from Isfahan University of Technology, Isfahan, Iran in 2012, and the Ph.D. degree from Ferdowsi University of Mashhad, Mashhad, Iran in 2019, both in electrical engineering. Since 2022, he has been collaborating with the Laboratory for Electric Drive Application and Research (LEDAR) at Toronto Metropolitan (formerly Ryerson) University in Toronto, Canada as a Postdoctoral Fellow. His current research interests include control of high-performance drives, power electronics, renewable energy technology, and applied nonlinear control.